2011 IEEE International Conference on Robotics and Automation
Shanghai International Conference Center
May 9-13, 2011, Shanghai, China

Maximizing Dexterous Workspace and Optimal Port Placement of a Multi-Arm Surgical Robot

Zhi Li, Daniel Glozman, Dejan Milutinovic and Jacob Rosen

Abstract— **Surgical procedures are traditionally performed by two or more surgeons along with staff nurses. One surgeon serves as the primary surgeon and the other serves as his/her assistant. Surgical robotics have redefined the dynamics in which the two surgeons interact with each other and with the surgical site. Raven IV is a new generation of the surgical robot system having four articulated robotic arms in a spherical configuration, each holding an articulated surgical tool. The system allows two surgeons to teleoperate the Raven IV collaboratively from two remote sites. The current research effort aims to configure the link architecture of each robotic arm, along with the position (port placement) and orientation of the Raven IV with respect to the patient, in order to optimize the common workspace reachable by all four robotic arms. The simulation results indicate that tilting the base of the robotic arms in the range of -20 to 20 deg while moving the ports closer together up to 50 mm apart leads to a preferred circular shape of the common workspace with an isotropy value of 0.5. A carefully configured system with multiple surgical robotic arms will enhance the interactive performance of the two surgeons.**

I. Introduction

Surgical procedures are traditionally performed by two or more individuals, along with staff nurses. With the introduction of a surgical robot into the operating room, the dynamics between the primary and assisting srugeons changed significantly. The primary surgeon, who controls the surgical robot, is immersed in a surgical console and is physically removed from the patient, while the assistant is usually locate next to the patient and hold another set of surgical tools. Raven IV (Figure 1) is a new generation of surgical robotic systems that includes four articulated arms. It allows two surgeons to collaborate using two surgical consoles that are located either next to the patient or at two remote locations. Raven IV is the second generation of Raven I [1]-[12]. The kinematic optimization of Raven I was based on the analysis of the workspace of a single arm [10], [11]. Other previous research efforts mainly focused on the design of port placement for cardiac procedures while using several existing robotic arm architectures such as the Zeus [13], [14] or DaVinci [15], [16] or a similar four bar mechanism [17] inserted between the ribs. With the introduction of four robotic arms, a new optimization approach is required for designing the size and the shape of the common workspace of the four robotic arms while ensuring the kinematic performance of each robotic arm. The scope of this research effort is a kinematic optimization of the surgical robotic arms in terms of their structural configurations as well as their positions (port placement) and orientations with respect to the patient.

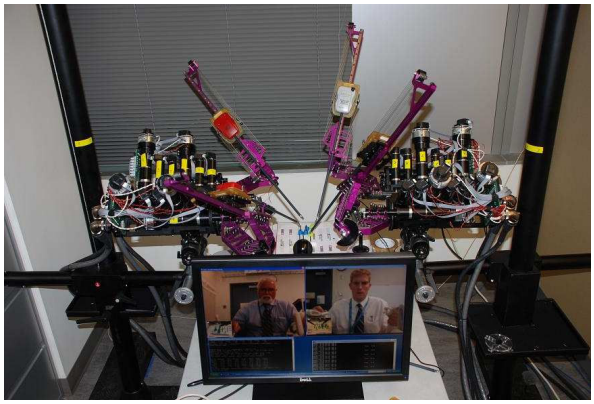

(a)

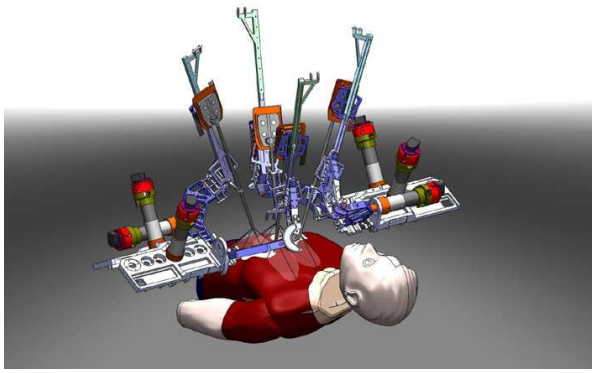

(b)

Fig. 1. Raven IV Surgical Robot System: (a) Hardware integration. (b) CAD rendering of the four Raven IV arms interacting with the patient; operation area is covered by the conical common workspace.

Z. Li (zhil@soe.ucsc.edu) and J. Rosen (rosen@soe.ucsc.edu) are with Department of Computer Engineering, University of California, Santa Cruz, CA 95064, USA

D. Milutinovic (Dejan@soe.ucsc.edu) is with the Department of Applied Mathematics & Statistics, University of California, Santa Cruz, CA 95064, USA

D. Glozman (daniel@glozman.org) was with the Department of Computer Engineering, University of California, Santa Cruz, CA 95064, USA. He is currently with Medtronic Ventor, Isrel

Bionics Lab URL: http://bionics.soe.ucsc.edu/

II. Kinematics of Raven IV

A. Direct Kinematics of the Raven IV Arms

The Raven IV surgical robot system consists of two pairs of surgical robotic arms. The pairs are mirror images of each other, which results in symmetric kinematics. Each arm has seven degrees of freedom (DOFs): six DOFs for positioning

and orienting the end-effector and one for opening and closing the end-effector.

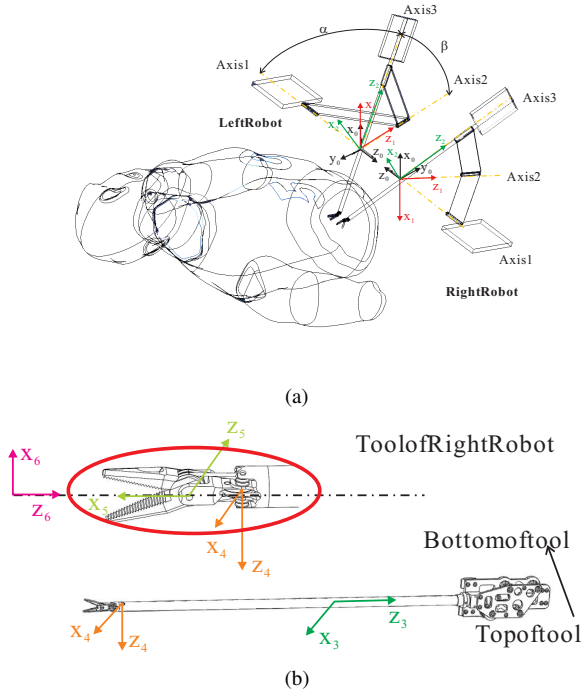

Fig. 2. Reference Frame of the Raven IV surgical robot system: (a) arms and (b) tools.

The base frame is located at the converging center of the spherical mechanism formed by the first three links of a Raven IV arm (Figure 2(a)). The Denavit-Hartenberg (DH) Parameters (Table I) are derived in the standard method defined by [18].

The direct kinematics can be derived from Table I, for the left and right arms respectively. Note that $sin\theta_i$ is denoted as s_i, $cos\theta_i$ is denoted as c_i, $sin\alpha_i$ is denoted as $s\alpha_i$, $cos\alpha_i$ is denoted as $c\alpha_i$.

TABLE I
DENAVIT-HARTENBERG PARAMETERS FOR RAVEN IV ARMS (STANDARD METHOD).

Robot	$i-1$	i	α_i	a_i	d_i	θ_i
Left Robot (1,3)	0	1	$\pi-\alpha$	0	0	$\theta_1(t)$
	1	2	$-\beta$	0	0	$-\theta_2(t)$
	2	3	0	0	0	$\pi/2-\theta_3(t)$
	3	4	$-\pi/2$	0	$d_4(t)$	0
	4	5	$\pi/2$	a_5	0	$\pi/2-\theta_5$
	5	6	$-\pi/2$	0	0	$\pi/2+\theta_6$
Right Robot (2,4)	0	1	$\pi-\alpha$	0	0	$\pi-\theta_1(t)$
	1	2	$-\beta$	0	0	$\theta_2(t)$
	2	3	0	0	0	$\pi/2+\pi+\theta_3(t)$
	3	4	$-\pi/2$	0	$d_4(t)$	0
	4	5	$-\pi/2$	a_5	0	$\pi/2+\theta_5$
	5	6	$-\pi/2$	0	0	$\pi/2-\theta_6$
Range	$\theta_1 \in [0°, 90°]$					$\theta_2 \in [20°, 140°]$
	$\theta_3 \in [-86°, 86°]$					$d_4 \in [0, 250]$ mm
	$\theta_5 \in [-86°, 86°]$					$\theta_6 \in [-86°, 86°]$

The direct kinematics is defined as the position and the orientation of the end-effector with respect to the base frame:

$$ {}^0_6T = {}^0_1T \cdot {}^1_2T \cdot {}^2_3T \cdot {}^3_4T \cdot {}^4_5T \cdot {}^5_6T = \begin{bmatrix} r_{11} & r_{12} & r_{13} & P_x \\ r_{21} & r_{22} & r_{23} & P_y \\ r_{31} & r_{32} & r_{33} & P_z \\ 0 & 0 & 0 & 1 \end{bmatrix} \quad (1) $$

B. Inverse Kinematics of the Raven IV Arms

Given the position and orientation of the end-effector of a Raven IV arm, the six DOFs for positioning and orienting the end-effector can be determined by resolving inverse kinematics analytically. To ensure the reachability of the given point, the resolution of the inverse kinematics should satisfy the joint limits in Table I. Equation (1) describes the homogeneous transformation of the kinematics of a Raven IV arm.

Hence, ${}^6_0T$ can be determined as the inverse of ${}^0_6T$ such that

$$ {}^6_0T = \begin{bmatrix} r'_{11} & r'_{12} & r'_{13} & P_{xinv} \\ r'_{21} & r'_{22} & r'_{23} & P_{yinv} \\ r'_{31} & r'_{32} & r'_{33} & P_{zinv} \\ 0 & 0 & 0 & 1 \end{bmatrix} \quad (2) $$

where for the left Robot,

$$ \begin{aligned} P_{xinv} &= (-d_4c_5 + a_5)c_6 \\ P_{yinv} &= s_5d_4 \\ P_{zinv} &= (-d_4c_5 + a_5)s_6 \end{aligned} \quad (3) $$

and for the right robot,

$$ \begin{aligned} P_{xinv} &= (d_4c_5 - a_5)c_6 \\ P_{yinv} &= s_5d_4 \\ P_{zinv} &= (-d_4c_5 + a_5)s_6 \end{aligned} \quad (4) $$

Let us define P_{inv} as:

$$ \begin{aligned} P^2_{inv} &= (P^2_{xinv} + P^2_{yinv} + P^2_{zinv}) \\ &= (d_4c_5 - a_5)^2c_6^2 + s_5^2d_4^2 + (-d_4c_5 + a_5)^2s_6^2 \\ &= (a_5 - d_4c_5)^2 + s_5^2d_4^2 \\ &= a_5^2 - 2a_5d_4c_5 + d_4^2c_5^2 + s_5^2d_4^2 \\ &= a_5^2 - 2a_5d_4c_5 + d_4^2 \end{aligned} \quad (5) $$

which gives:

$$ c_5^2 = \left(\frac{a_5^2 + d_4^2 - P^2_{inv}}{2a_5d_4}\right)^2 \quad (6) $$

Note that both (3) and (4) lead to

$$ c_5^2 = 1 - s_5^2 = 1 - (P_{yinv}/d_4)^2 \quad (7) $$

Hence,

$$ 1 - \left(\frac{P_{yinv}}{d_4}\right)^2 = \left(\frac{a_5^2 + d_4^2 - P^2_{inv}}{2a_5d_4}\right)^2 \quad (8) $$

Equation (8) satisfies both the left robot and the right robot and therefore leads to four possible solutions to d_4 as:

$$d_{41} = \sqrt{a_5^2 + P_{inv}^2 + 2a_5\sqrt{(P_{inv}^2 - P_{yinv}^2)}} \quad (9)$$

$$d_{42} = -\sqrt{a_5^2 + P_{inv}^2 + 2a_5\sqrt{(P_{inv}^2 - P_{yinv}^2)}} \quad (10)$$

$$d_{43} = \sqrt{a_5^2 + P_{inv}^2 - 2a_5\sqrt{(P_{inv}^2 - P_{yinv}^2)}} \quad (11)$$

$$d_{44} = -\sqrt{a_5^2 + P_{inv}^2 - 2a_5\sqrt{(P_{inv}^2 - P_{yinv}^2)}} \quad (12)$$

out of which only (12) is acceptable for both the left and right arm given the constrain in Table I.

θ_6 can by resolved as:

$$s_6 = P_{zinv}/(-d_4c_5 + a_5) \quad (13)$$

for the left robot,

$$c_6 = P_{xinv}/(-d_4c_5 + a_5) \quad (14)$$

and for the right robot,

$$c_6 = -P_{xinv}/(-d_4c_5 + a_5) \quad (15)$$

$$\theta_6 = Atan2(s_6, c_6) \quad (16)$$

θ_5 can be resolved as:

$$s_5 = P_{yinv}/d_4 \quad (17)$$

$$c_5 = \sqrt{1 - s_5^2} \quad (18)$$

$$\theta_5 = Atan2(s_5, c_5) \quad (19)$$

Given the solution of d_4, θ_5 and θ_6, we can compute

$$ {}^0_3T = {}^0_1T \cdot {}^1_2T \cdot {}^2_3T = {}^0_6T \cdot [{}^3_4T \cdot {}^4_5T \cdot {}^5_6T]^{-1} = \begin{bmatrix} a_{11} & a_{12} & a_{13} & a_x \\ a_{21} & a_{22} & a_{23} & a_y \\ a_{31} & a_{32} & a_{33} & a_z \\ 0 & 0 & 0 & 1 \end{bmatrix} \quad (20)$$

where

$$a_{32} = s_2s_\alpha c_3 + (c_2s_\alpha c_\beta + c_\alpha s_\beta)s_3 \quad (21)$$

$$a_{33} = c_2s_\alpha s_\beta - c_\alpha c_\beta \quad (22)$$

θ_2 can be resolved as:

$$c_2 = \frac{c_\alpha c_\beta + a_{33}}{s_\alpha s_\beta} \quad (23)$$

$$s_2 = \sqrt{1 - c_2^2} \quad (24)$$

$$\theta_2 = Atan2(s_2, c_2) \quad (25)$$

Let us define $a = s_2s_\alpha$ and $b = c_2s_\alpha c_\beta + c_\alpha s_\beta$. Equation (21) becomes

$$a_{32} = ac_3 + bs_3 \quad (26)$$

and a, b and a_{32} are known. Equation (26) can be solved with the tangent-of-the-half-angle substitutions (see Section 4.5 of [18]):

$$\theta_3 = 2Atan(\frac{b \pm \sqrt{a^2 + b^2 - a_{32}^2}}{a + a_{32}}) \quad (27)$$

Equation (26) can also be solved as (see C.10 of [18]):

$$\theta_3 = Atan2(b, a) \pm Atan2(\sqrt{a^2 + b^2 - a_{32}^2}, a_{32}) \quad (28)$$

Note that solutions only exist when $a^2 + b^2 - a_{32}^2 \geq 0$. Additionally, (27) requires $a + a_{32} \neq 0$; (28) requires $a_{32} \neq 0$ and $a \neq 0$.

An algorithm to check a_{13} ((29) and (30)) in (20) can be used to choose between the two possible solutions of θ_3. For the left robot,

$$a_{13} = -s_2s_\alpha s_3 + c_2s_\alpha c_3c_\beta + c_\alpha c_3s_\beta \quad (29)$$

For the right robot,

$$a_{13} = s_2s_\alpha s_3 - c_2s_\alpha c_3c_\beta - c_\alpha c_3s_\beta \quad (30)$$

Given the solution for θ_2 and θ_3, θ_1 can be determined by:

$$ {}^0_1T = {}^0_6T \cdot [{}^3_4T \cdot {}^4_5T \cdot {}^5_6T]^{-1}[{}^1_2T \cdot {}^2_3T]^{-1} = \begin{bmatrix} b_{11} & b_{12} & b_{13} & b_x \\ b_{21} & b_{22} & b_{23} & b_y \\ b_{31} & b_{32} & b_{33} & b_z \\ 0 & 0 & 0 & 1 \end{bmatrix} \quad (31)$$

with $s_1 = b_{11}$, $c_1 = b_{21}$ for the left robot, $s_1 = b_{11}$, $c_1 = b_{21}$ for the right robot and

$$\theta_1 = Atan2(s_1, c_1) \quad (32)$$

To the best of our knowledge, the inverse kinematics of the Raven IV surgical system that involves six degrees of freedom has not been studied before.

III. Optimization of the Common Workspace

A. The Common Workspace

All four Raven IV arms are arranged with respect to each other as depicted in Figure 3. Each gray bar represents the base of one arm. The magenta and the cyan bars represents the first and second links respectively. These four Raven IV arms can reach a common volume in 3D space. For the purpose of optimizing the system, a reference 2D plane was defined inside the patient 150 mm below the plain including the ports of the four arms.

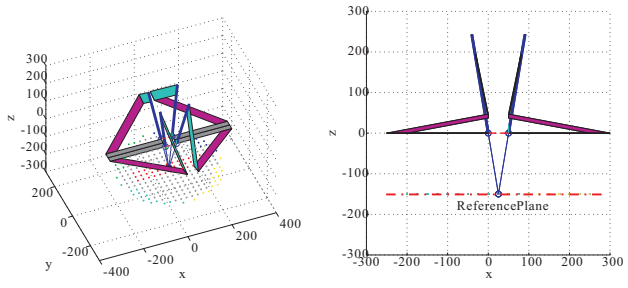

(a) (b)

Fig. 3. The common workspace projected onto the reference plane: (a) 3D view; (b) projection onto x-z plane. For each Raven IV arm, the gray bar represents its base. The magenta and the cyan bars represent the first and second link respectively.

B. Area-Circumference Ratio

The optimized common workspace is expected to have the largest circular area possible as opposed to an elliptical area. Mathematically, the area and shape of the common workspace can be collectively evaluated by the ratio between the area and the circumference ratio of the common workspace ς, which is defined as

$$\varsigma = \frac{Area}{Circumference} \tag{33}$$

According to the **isoperimetric inequality**, a circle has the largest possible area among all the shapes with the same circumference. The Area-Circumference ratio of a circle ς_c is proportional to its radius r:

$$\varsigma_c = \frac{\pi r^2}{2\pi r} = \frac{r}{2} \tag{34}$$

Practically, the common workspace has an amorphic shape that can not be expressed analytically. However, maximizing ς, i.e. $max(\varsigma)$, will result in the common workspace that is as close as possible to a circle.

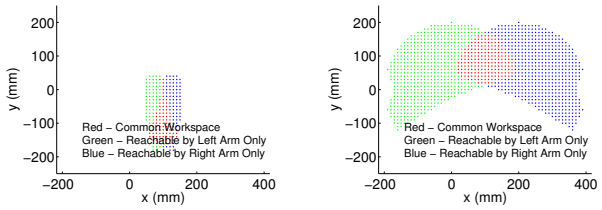

(a) (b)

Fig. 4. Example of common workspace of two Raven IV arms: (a) $\alpha = 65°$, $\beta = 15°$, $\varsigma = 2.23$; (b) $\alpha = 65°$, $\beta = 80°$, $\varsigma = 4.48$.

Figure 4 presents two common workspace of two Raven IV arms resulting from different link lengths. The common workspace depicted in Figure 4(b) (with $\varsigma = 4.48$) is preferable compared to the workspace illustrated in Figure 4(a).

C. Mechanism Isotropy

Isotropy is a performance measure in the range of $[0, 1]$ where 0 represents singular configuration of the mechanism and 1 represents the mechanism's ability to move equally in all directions. The isotropy is defined based on the Jacobian matrix $\mathbf{J}$ as one over the condition number of the Jacobian matrix.

$$Iso = \frac{1}{Condition\ number\ of\ \mathbf{J}} \tag{35}$$

The Jacobian matrix is derived analytically by using the velocity propagation method in which the angular velocity is propagated as:

$${}^{i+1}\omega_{i+1} = {}^{i+1}_{i}R\,{}^{i}\omega_i + \dot{\theta}_{i+2}\hat{Z}_{i+1} \tag{36}$$

and the linear velocity is propagated as:

$${}^{i+1}\mathbf{v}_{i+1} = {}^{i+1}_{i}R({}^{i}\omega_i \times {}^{i}P_{i+1} + {}^{i}\mathbf{v}_i) + \dot{d}_{i+2}\hat{Z}_{i+1} \tag{37}$$

Note that for a prismatic joint, $\dot{\theta}_{i+1} = 0$ in (36); for a revolute joint, $\dot{d}_{i+1} = 0$ in (37).

Since the mass and dimension of the end-effector is negligible comparing to the first three links of the Raven IV arms, this analytical derivation of the Jacobian includes only the positioning of the wrist of the Raven IV arm, i.e., θ_1, θ_2 and d_4. Therefore, DH parameters in Table I are modified to rule out the non-relevant DOFs: (1) $\theta_3 = 0$; (2) $\alpha_4 = 0$; (3) DH parameters relevant to joint 5 and joint 6 are not considered and therefore are all set to zero.

By velocity propagation, the angular velocity of the tool wrist for the left arm is:

$${}^{3}\mathbf{v}_3 = \begin{bmatrix} c_2c_\beta s_\alpha\dot{\theta}_1 + s_\beta c_\alpha\dot{\theta}_1 - s_\beta\dot{\theta}_2 \\ s_2 s_\alpha\dot{\theta}_1 \\ c_2 s_\beta s_\alpha\dot{\theta}_1 - c_\beta c_\alpha\dot{\theta}_1 + c_\beta\dot{\theta}_2 \end{bmatrix} \tag{38}$$

and for the right arm is:

$${}^{3}\mathbf{v}_3 = \begin{bmatrix} -c_2c_\beta s_\alpha\dot{\theta}_1 - s_\beta c_\alpha\dot{\theta}_1 + s_\beta\dot{\theta}_2 \\ s_2 s_\alpha\dot{\theta}_1 \\ c_2 s_\beta s_\alpha\dot{\theta}_1 - c_\beta c_\alpha\dot{\theta}_1 + c_\beta\dot{\theta}_2 \end{bmatrix} \tag{39}$$

The linear velocities of the tool's wrist are the same for both the left arm and right arm, which is:

$${}^{3}\mathbf{v}_3 = \begin{bmatrix} 0 \\ 0 \\ \dot{d}_4 \end{bmatrix} \tag{40}$$

Therefore, the Jacobian matrix for the left robot is:

$${}^{3}\mathbf{J} = \begin{bmatrix} c_2c_\beta s_\alpha + s_\beta c_\alpha & -s_\beta & 0 \\ s_2 s_\alpha & 0 & 0 \\ c_2 s_\beta s_\alpha - c_\beta c_\alpha & c_\beta & 1 \end{bmatrix} \tag{41}$$

and for the left robot is:

$$ {}^3\mathbf{J} = \begin{bmatrix} -(c_2c_\beta s_\alpha + s_\beta c_\alpha) & s_\beta & 0 \\ s_2 s_\alpha & 0 & 0 \\ c_2 s_\beta s_\alpha - c_\beta c_\alpha & c_\beta & 1 \end{bmatrix} \quad (42) $$

The resulting Jacobian matrix has a unit vector corresponding to the prismatic joint along the z-axis of Frame 4. Therefore, the mechanism isotropy only depends on the 2×2 top left sub-matrix of the Jacobian, denoted as ${}^3\mathbf{J}_s$.

IV. Simulation

A. Cost Function

The common workspace is to be optimized from the following four perspectives: (1) the the Area-Circumference ratio (ς) is maximized given bounded isotropy values; (2) The average isotropy of the common workspace is maximized; (3) the minimum isotropy of the common workspace is maximized; and (4) the dimension of the robot arm is minimized, which results in a stiffer structure. With the above considerations, the cost function of the optimization of the common workspace is defined as:

$$ C = \max_{(\alpha,\beta,\phi_x,\phi_y,\phi_z,b_x,b_y)} \{ \frac{\varsigma \cdot \sum Iso \cdot Iso_{min}}{\alpha^3 + \beta^3} \} \quad (43) $$

Where $\sum Iso$ denotes the sum of the actual isotropy of the points in the common workspace, Iso_{min} denotes the minimum isotropy required in the common workspace, and $\alpha^3 + \beta^3$ represents the stiffness of the structure, since the stiffness of the link is inversely proportional to the cubic power of the dimension.

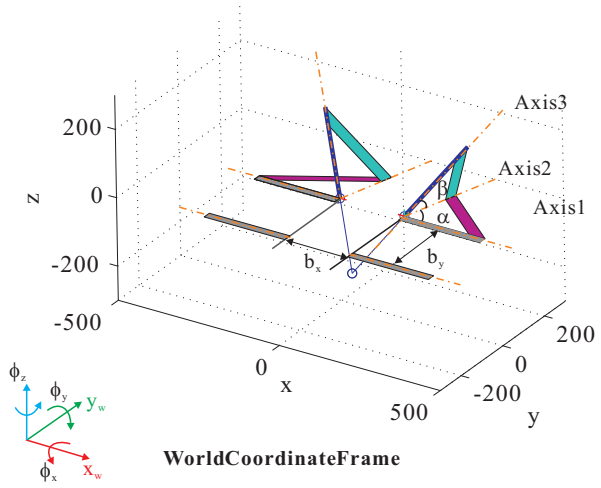

Fig. 5. Parameters for the optimization of the common workspace.

Equation (43) intends to maximize the cost function by choosing the link length of the first two links α and β, the distance between the ports, the base orientation of the arms, and the minimum isotropy required in the workspace: (1) the α between the Axis 1 and Axis 2, and the β between Axis 2 and Axis 3; (2) the base orientation are about X_w, Y_w and Z_w axes of the world coordinate frame respectively, i.e. ϕ_x, ϕ_y and ϕ_z; and (3) the port spacing b_x and b_y is the horizontal distance between the bases of the Raven IV arms, measured along X_w and Y_w respectively; (4) Iso_{min} is the minimum isotropy required in the common workspace.

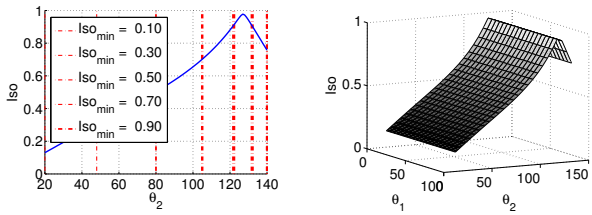

(a) (b)

Fig. 6. ((a) Range of θ_2 affected by different Iso_{min} ($\alpha = 55°$,$\beta = 40°$). (b) Note that given a specified θ_2, Iso are the same for all value of θ_1.

This section intends to find the common workspace of four cooperative Raven IV Arms by **brute force** simulation. The cost function for the optimization involves adjustable parameters relevant to the link lengths, the port spacing and the base orientation, and the minimum required isotropy.

B. Isotropy Performance

Limiting the minimum isotropy performance Iso_{min} has a significant effect on the resulting optimized common workspace. Since θ_1 and d_4 are not involved in the analytical expression of the Jacobian, Iso_{min} only depends on the range of θ_2 and therefore it narrows down the workspace of each Raven IV arm, as shown in Figure 6.

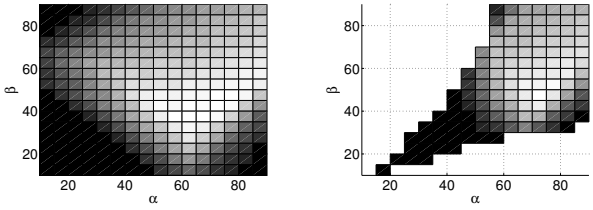

(a) (b)

Fig. 7. Distribution of ς for different Iso_{min}. (a) For $Iso_{min} = 0$, $\varsigma_{max} = 6.64$ when $\alpha = 80°$, $\beta = 40°$; (b) For $Iso_{min} = 0.5$, $\varsigma_{max} = 6.55$ when $\alpha = 70°$, $\beta = 35°$.

C. All-in-One Optimization

The workspace of the Raven IV surgical robot system can be further optimized by adjusting the base orientation and port spacing. Simulation in this section explores all seven parameters in (43) within the limited ranges defined by Table II to find the preferred value for each parameter.

The results show that the Raven IV arms should be arranged as depicted in Figure 8(a) to achieve the most optimal common workspace (Figure 8(b)).

V. Conclusion

We derived the direct kinematics and resolved the inverse kinematics of the Raven IV surgical robot system. The Area-Circumference ratio ς is used to evaluate the geometric

TABLE II

PARAMETER RANGES AND PREFERRED VALUES FOR THE OPTIMIZATION OF THE RAVEN IV SURGICAL ROBOT SYSTEM.

	Range	Optimal Value	Resolution
α	$[5°, 90°]$	$85°$	$20°$
β	$[5°, 90°]$	$65°$	$20°$
ϕ_x	$[-20°, 20°]$	$20°$	$10°$
ϕ_y	$[-20°, 20°]$	$10°$	$10°$
ϕ_z	$[-20°, 20°]$	$-20°$	$10°$
b_x	$[50, 200]$ (mm)	100 (mm)	50 (mm)
b_y	$[50, 200]$ (mm)	50 (mm)	50 (mm)
Iso_{min}	$[0.1, 0.9]$	0.5	0.2
Result	$C_{max} = 526.3$ for Iso_{min} =0.5		

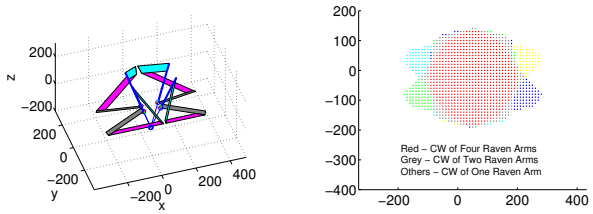

(a) (b)

Fig. 8. (a) Raven IV surgical robot system and (b) its optimized workspace.

properties of the common workspace of the four Raven IV arms. Furthermore, bounding mechanism isotropy ensures high performance of each individual arm. The analytical derivation shows that: (1) the mechanism isotropy performance of a Raven IV arm depends on a 2×2 sub-matrix in the 3×3 Jacobian matrix for the end-effector positioning (i.e. θ_1, θ_2 and d_4); (2) setting the minimum isotropy value narrows down the working range of Joint 2 of each Raven IV arm and therefore affects the geometric properties of the common workspace.

Based on its kinematic properties, the common workspace of the four Raven IV arms is optimized by adjusting the link lengths, the port spacing and the base orientations within practical ranges of each parameter. The four Raven IV arms will have a optimized common workspace with the cost function that involves the Area-Circumference ratio and the mechanism isotropy performance if the ports are spaced at $b_x = 100$ mm and $b_y = 50$ mm, and the bases are rotated about the X-axis by $\phi_x = 20°$, about the Y-axis by $\phi_y = 10°$ and about the Z-axis by $\phi_z = -20°$ in the world coordinate system.

REFERENCES

[1] M. Lum, D. C. W. Friedman, G. Sankaranarayanan, H. King, K. F. II, R. Leuschke, B. Hannaford, J. Rosen, and M. N. Sinanan, "The raven - a multidisciplinary approach to developing a telesurgery system," *Int. Journal of Robotic Research, Special Issue:Medical Robotics Part I*, vol. 28, no. 9, pp. 1183–1197, Sept. 2009.

[2] M. Lum, J. Rosen, T. S. Lendvay, M. N. Sinanan, and B. Hannaford, "Effect of time delay on telesurgical performance," in *IEEE Int. Conf. on Robotics & Automation*, Kobe, Japan, May 2009, pp. 4246–4252.

[3] M. J. Lum, J. Rosen, H. King, D. Friedman, T. Lendvay, A. S. Wright, M. N. Sinanan, and B. Hannaford, "Teleopeartion in surgical robotics - network latency effects on surgical performance," in *31th Annual Int. Conf. of the IEEE Engineering in Medicine and Biology Society EMBS*, Minneapolis, MN, USA, Sept. 2009, pp. 6860–6863.

[4] M. J. Lum, J. Rosen, T. Lendvay, A. S. Wright, M. N. Sinanan, and B. Hannaford, "Telerobotic fundamentals of laparoscopic surgery (fls): Effects of time delay - pilot study," in *30th Annual Int. Conf. of the IEEE Engineering in Medicine and Biology Society EMBS*, Vancouver, BC, Canada, Aug. 2008, pp. 5597–5600.

[5] H. Brett, C. Doarn, J. Rosen, B. Hannaford, and T. J. Broderick, "Evaluation of unmanned airborne vehicles and mobile robotic telesurgery in an extreme environment," *Telemedicine and e-Health*, vol. 14, no. 6, pp. 534–544, July 2008.

[6] M. Lum, D. Friedman, G. Sankaranarayanan, H. King, A. Wright, M. Sinanan, T. Lendvay, J. Rosen, and B. Hannaford, "Objective assessment of telesurgical robot systems: Telerobotic fls," in *Medicine Meets Virtual Reality (MMVR 16)*, Long Beach, CA, USA, Jan. 2008, pp. 263–265.

[7] G. Sankaranarayanan, B. Hannaford, H. King, S. Ko, M. Lum, D. F. J. Rosen, and B. Hannaford, "Portable surgery master station for mobile robotic surgery," in *Proc. of the 1st Int. conference on Robot Communication and Coordination*, Athens, Greece, Oct. 2007.

[8] M. Lum, D. Friedman, H. King, R. Donlin, G. Sankaranarayanan, T. Broderick, M. Sinanan, J. Rosen, and B. Hannaford, "Teleoperation of a surgical robot via airborne wireless radio and transatlantic internet links," in *The 6th Int. Conf. on Field and Service Robotics*, Chamonix, France, July 2007.

[9] M. Lum, J. Rosen, H. King, D. Friedman, G. Donlin, G. Sankaranarayanan, B. Harnett, L. Huffman, C. Doarn, T. Broderick, and B. Hannaford, "Telesurgery via unmanned aerial vehicle (uav) with a field deployable surgical robot," in *Proc. of Medicine Meets Virtual Reality (MMVR 15)*, Long Beach, CA, USA, Feb. 2007.

[10] M. Lum, J. Rosen, M. Sinanan, and B. Hannaford, "Optimization of spherical mechanism for a minimally invasive surgical robot: Theoretical and experimental approaches," *IEEE Transactions on Biomedical Engineering*, vol. 53, no. 7, pp. 1440–1445, July 2006.

[11] M. Lum, J. Rosen, M. Sinanan, and B. Hanaford, "Kinematic optimization of a spherical mechanism for a minimally invasive surgical robot," in *IEEE Int. Conf. on Robotics & Automation*, New-Orleans, USA, Apr. 2004, pp. 829–834.

[12] J. Rosen, M. Lum, M. Sinanan, and B. Hannaford, "Raven: Developing a surgical robot from a concept to a transatlantic teleoperation experiment," in *Surgical Robotics, Systems, Applications, and Visions, 1st edition*, R. M. Satava, Ed. Springer, 2011, pp. 159–197.

[13] J. Cannon, J. Stoll, S. Selha, P. Dupont, R. Howe, and D. Torchiana, "Port placement planning in robot-assisted coronary artery bypass," *IEEE Transactions on Robotics & Automation*, vol. 19, no. 5, pp. 912–917, Oct. 2003.

[14] S. Selha, P. Dupont, R. Howe, and D. Torchiana, "Dexterity optimization by port placement in robot-assisted minimally invasive surgery," in *2001 SPIE Int. Sym. on Intelligent Systems & Advanced Manufacturing*, Newton, MA, USA, Oct. 2001.

[15] L. Trejos and R. Patel, "Port placement for endoscopic cardiac surgery based on robot dexterity optimization," in *Proc. of the 2005 IEEE Int. Conf. on Robotics & Automation*, Barcelona, Spain, May 2005.

[16] R. Bauernschmitt, M. Feuerstein, J. Traub, E. Schirmbeck, G. Klinker, and R. Lange, "Optimal port placement and enhanced guidance in robotically assisted cardiac surger," *Surg Endosc*, vol. 21, pp. 684–687, 2007.

[17] J. Li, S. Wang, X. Wang, and C. He, "Optimization of a novel mechanism for a minimally invasive surgery robot," *Int. Journal Medicine Robotics Computer Assist Surgery*, vol. 6, pp. 83–90, 2010.

[18] J. Craig, *Introduction to Robotics: Mechanics and Control, 3rd edition*. Prentice Hall, 2003, ch. 1.